CHAPTER 5

Pluronic mediated silica nanoparticles with chitosan as composite for gas adsorption

5.1: Introduction

Agriculture wastes are renewable, biocompatible, and abundant on earth, and their proper utilization in the production of bio-based products has been of keen interest nowadays for environmentally friendly and sustainable chemistry [1,2]. Mostly agriculture waste of the world are corn cobs (CC), rice husk (RH), peanut shell (PS), wheat straw (WS), and sugarcane bagasse (SB) [3,4]. In addition to lignocelluloses, agriculture waste such as RH, PS, SB also contain a good amount of silica (SiO_2), making them valuable renewable sources for production of silica nanoparticles (SiO_2NPs) [5-8].

India is the world's second-largest peanut producer (13%, 6650 millionMT) and the main purpose of peanuts is to produce rich protein content, oil content, and fiber content [1, 9]. However, many PS are not systematically used and are often either burned or buried, resulting in millions of tons of peanut shell ash (PSA) production per year. Mostly PSA is disposed of in dumps, causing pollution to the environment and human health as a large amount of SiO_2 in the form of dust is present in the crystalline form [3]. Therefore, the use of PSA for development of SiO_2NPs is fundamental. SiO_2NPs have a wide range of applications, including chromatographic columns, paints, catalysts, fuel cell membranes, biopolymers, and adsorbents, among others [10-16].

The involvement of polymers plays a key role in the synthesis of SiO_2NPs to precisely control the size, shape, stability through steric or electrostatic means, preventing aggregation, and introducing functional groups that improve compatibility with other materials or biological systems [17, 18]. The polymer-assisted SiO_2NPs have found extensive applications, including targeted drug delivery systems that enhance therapeutic effectiveness and minimize side effects, catalysts or catalyst supports in chemical reactions due to their high surface area and enhanced reactivity, and components in sensors that offer high sensitivity and specificity. Not only are that SiO_2NPs used in composite materials to enhance optical, thermal, andmechanicalproperties [19, 20].

Modification of SiO_2NPs using chitosan polymer put forward the advanced material science, combining the unique properties of chitosan, a natural biopolymer derived from chitin, with those of silica to create a multifunctional material with a broad range of applications in many fields, including biomedicine, environmental science, and engineering [21-23]. Chitosan is

familiar for its surface adhesion, high hydrophilicity, chemical stability, and improved antibacterial activity with biodegradability. Chitosan is a copolymer composed of glucose and amino-glucose units. It has three functional groups: 1° and 2° OH groups, $-NH_2$, and $-NHCOCH_3$. All these groups are favoring the formation of strong hydrogen bonds and good interaction with a variety of compounds [24]. With such functionality, chitosan contributes to the effective adsorption phenomenon and makes them useful as an adsorbent for the removal of many organic compounds. The synergistic combination of chitosan and SiO_2NPs results in a material that is not only biocompatible and environmentally friendly but also exhibits a large surface area and enhanced functionality, which are effective as green adsorbents for gas separation and removal of organic pollutants. Several studies have already successfully used chitosan-modified SiO_2NPs for the adsorption of organic pollutants [3, 13, 22].

In this context, Our work focuses on the following key contributions: (1) Synthesis of Pluronic mediated SiO_2NPs using the agriculture waste PSA and different biocompatible Pluronic surfactants (Polyethylene oxide-polypropylene oxide-polyethylene oxide triblock copolymers), (2) Modification of SiO_2NPs with chitosan coating; (3) Characterization of the developed chitosan-modified SiO_2NPs (Ch/SiO_2NPs) as a biosorbent using DLS, TEM, FE-SEM, EDX, XRD, TGA, FTIR, and BET analysis; and (4) Adsorption studies of gases (CO_2, CH_4, and N_2) using Ch/SiO_2NPs as a biosorbent through the interaction of Ch/SiO_2NPs biosorbent for better environmental applications.

5.2: Experimental section

5.2.1: Preparation of Pluronic mediated SiO_2NPs using peanut shell ash (PSA)

Scheme 5.1(a) shows the preparation of Pluronic mediated SiO_2NPs schematically. First, 350 g of PSA was added into 500 mL of 0.2 M HCl and stirred at 450 rpm for 3 h. The solid residue was then filtered, washed with deionized water, and dried overnight at 95°C. The smaller particles of dried PSA were collected using a molecular sieve of 0.50 mm. The PSA particles were mixed with solid NaOH at a 1:3 weight ratio and heated at 100 °C for 4 h, and again, the mixture was refluxed by adding 100 mL of deionized water for almost 4 h. After end of the reaction, the mixture was filtered, and the sodium silicate solution was collected.

Add slowly 20 mL of 5 wt% Pluronic solution in a round-bottom flask containing the 20 mL of sodium silicate solution with continuous stirring at 250 rpm. Various Pluronics were used to assess their effects on the size and shape of SiO_2NPs. The Pluronic-sodium silicate solution was neutralized (pH=7) gradually, adding drop by drop a 0.1 M sulfuric acid solution. The mixture was held at RT for 3 h to allow for the aging and stabilization of the SiO_2NPs and centrifuged for 30 min at 5000 rpm. The settled Pluronic mediated SiO_2NPs were collected and washed with ultrapure water. The collected solid SiO_2NPs were properly dried in a oven at 95 °C for 2 h.

5.2.2: Preparation of Chitosan-modified SiO_2NPs (Ch/SiO_2NPs)

Scheme 5.1(b) shows the schematic preparation of biosorbent Ch/SiO_2NPs. Firstly, dissolve various gm of chitosan (0.5, 1.0, 1.5, and 2.0 gm) in the 100 mL of 2% acetic acid solution. 10 gm of Pluronic mediated SiO_2NPs was added to a chitosan solution and stirred for almost 24 h to ensure that the chitosan fully penetrated and was evenly distributed throughout the pores of the SiO_2NPs (mesoporous). The mixture was then centrifuged at 4000 rpm, filtered, washed with ultrapure water, and dried in a vacuum oven at 50 °C for 6 h to get a solid powder of biosorbent Ch/SiO_2NPs.

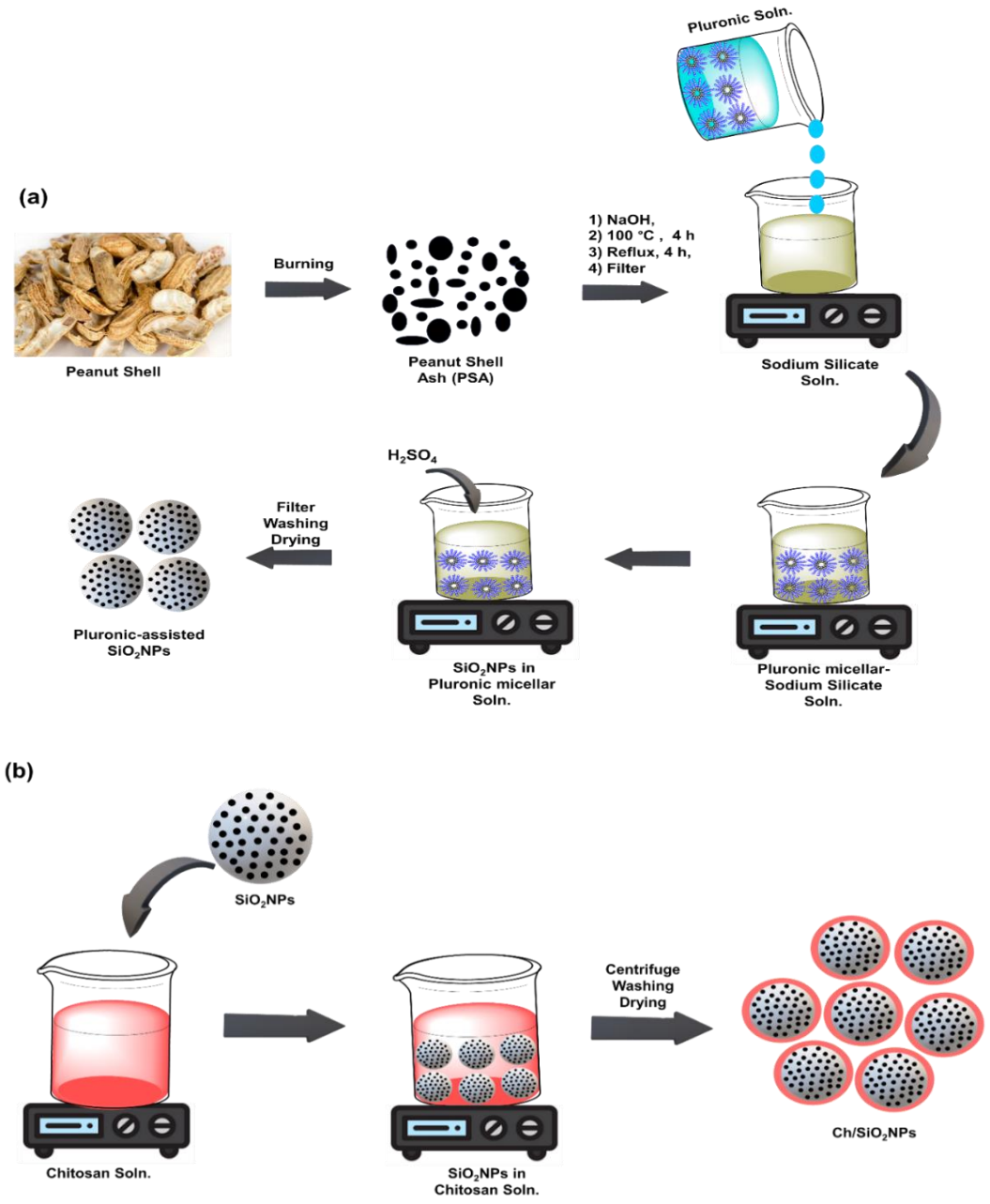

Scheme 5.1: (a) Preparation of Pluronic mediated SiO_2NPs from PSA and (b) development of Ch/SiO_2NPs biosorbent

5.2.3: Gas adsorption study

The isotherms of pure gases (99.99%) were experimentally determined on biosorbent Ch/SiO_2NPs. The adsorption isotherms of three important atmospheric gases, CO_2, CH_4, and N_2, were measured on a volumetric gas adsorption analyzer at 15°C, 25°C and 35°C. Prior to the

start of the experiment, the Ch/SiO_2NPs sample was degassed in a vacuum oven at 90°C for almost 4 h. The results were obtained through the process of introducing or extracting a predetermined amount of adsorbing gas into or out of a sample cell containing Ch/SiO_2NPs as the solid adsorbent. This process was conducted under controlled conditions of a constant temperature and relative pressures.

5.3: Results and Discussion

5.3.1: Structural and chemical properties of PSA and Pluronic mediated SiO_2NPs

As shown in Scheme 5.1, the PSA is produced by burning PS waste; this biomass has various impurities of salts and organic substances. To remove undesirable salts and organic impurities from PSA, it was treated with 0.2 M HCl. The solid residue of PSA was then filtered, washed with deionized water, and dried overnight at 95 °C. The smaller PSA particles were obtained using a molecular sieve with a 0.5 mm diameter [25]. PSA particles reacting with NaOH at 100°C for 4 h, which helps better in extracting a high amount of silicon successfully. This process increases silicon purity by eliminating other elements from the PSA. The resulting silicon, in the form of sodium silicate (Na_2SiO_3), is dissolved in water and then filtered. The filtrate of soluble silicate was kept for the preparation of SiO_2NPs. The 5 wt% aqueous solutions Pluronic was then added to the sodium silicate solution. Pluronic is a polymeric nonionic surfactant that forms micelles, which are nano-in-size and capable of controlling the size of the synthesized nanoparticles, preventing their aggregation, and also modifying their surfaces [26]. SiO_2NPs is achieved with hydrolysis (production of silanol group) and condensation (formation of siloxane) reactions using acid (H_2SO_4) in a micellar medium of Pluronic. When H_2SO_4 is added slowly, white solid particles start to form into the Pluronic micelles [27], which worked as nanoreactors for controlling the size of the SiO_2NPs. The solid Pluronic mediated SiO_2NPs can be removed by centrifugation, washed and dried for further characterization.

Here, the various Pluronics (F68, F127, L64 and, P123) were checked to prepare SiO_2NPs for understanding their role on particle sizes of Pluronic mediated SiO_2NPs. Figure 5.1 showed the particle sizes of SiO_2NPs using different-different Pluronics. As per the DLS results, the particle size of SiO_2NPs was found to be 63.3 nm without the use of Pluronic, while it decreased up to 22.3 nm when Pluronic micellar solution was applied in the preparation. The particle sizes of SiO_2NPs were 48.1 nm, 22.3 nm, 27.4 nm, and 28.8 nm using F68, F127, L64, and P123, respectively. The type of micelles and their sizes play asignificant role in controlling the rate of the condensation reaction and better acidic gelation for the development of nanoparticles. With high molecular weight and HLB, hydrophilic F127 micelles favored the lowest size (22.3 nm) of SiO_2NPs, while hydrophobic micelles of L64 and P123 showed quite higher particle sizes (27.4 and 28.8 nm).

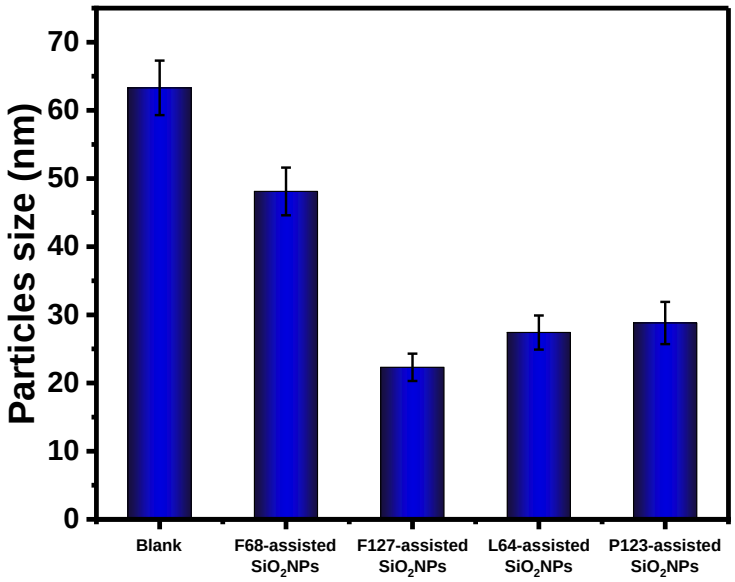

Figure 5.1: Particle size of Pluronic mediated SiO_2NPs

Here, it was clearly understood that the high ethylene oxide block segment in F127 prevented the aggregation of nanoparticles and effectively mediated the hydrolysis and condensation process of sodium silicate to SiO_2NPs formation when acid was added. It was clearly noticed that the adsorption scale up with the degree of polymerization i.e. molecular weight of Pluronic [28]. In compare to development of SiO_2NPs reported from various agriculture wastes, Pluronic mediated SiO_2NPs synthesized from PS in this work shown promising approach as produces quite smaller in sizes (Table 5.1). To compare the purity, particle sizes, and morphology of SiO_2NPs with PSA, F127 mediated SiO_2NPs was taken as Pluronic mediated SiO_2NPs. The elemental composition of both PSA and Pluronic mediated SiO_2NPs was determined using EDX analysis, as shown in Table 5.2 and Figure 5.2. The findings indicated that the SiO_2 content in PSA was 63.02 wt%, while in the Pluronic mediated SiO_2NPs, it was 92.84 wt%.

The results clearly indicated the notable improvement in the purity of SiO_2NPs. The results of the elements clearly showed that the amounts of MgO, P_2O_5, K_2O, CuO, and ZnO were quite diminishing in Pluronic mediated SiO_2NPs in comparison to PSA. Elements like Na_2O, CaO, FeO, SO_3, and Al_2O_3, which were present in the PSA, found absent in the Pluronic mediated SiO_2NPs, confirming the high purity of the SiO_2NPs in the EDX analysis.

Table 5.1: Particle size of SiO_2NPs produced from various agriculture wastes.

Agriculture waste	Particle size, nm	References
Peanut shell	100 to 350	Shahi et al [1]
Rice-husk	181.2 to 294.7	Carmona et al [6]
Rice straw	70 to 100	Uda et al [29]
Sugarcane bagasse	100	Rovani et al [30]
Barley-husk-grass	102-145	Akhayere et al [31,32]
Palm shell	50-98	Imoisili et al [33]
Peanut shell	18 to 48.1	Pluronic-assisted SiO_2NPs (This work)

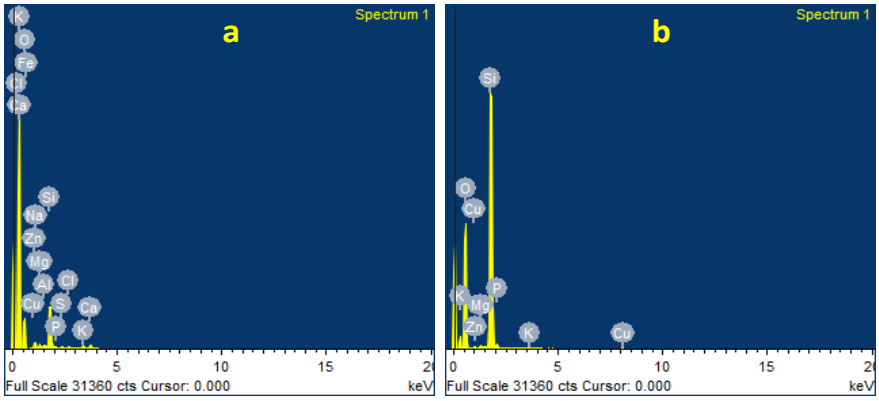

Figure 5.2: EDX spectra of PSA and Pluronic mediated SiO_2NPs.

Table 5.2: The weight percentages of elements in PSA and Pluronic mediated SiO_2NPs were measured using EDX analysis.

Elements	PSA (wt%)	SiO_2NPs (wt%)
SiO_2	63.02	92.84
MgO	4.96	0.86
P_2O_5	3.15	2.72
K_2O	3.64	0.17
CuO	3.14	2.36
ZnO	2.07	1.05
CaO	4.87	-
Na_2O	6.75	-
Al_2O_3	2.31	-
SO_3	3.54	-
FeO	0.98	-

Figure 5.3 shows the SEM and TEM images of PSA and Pluronic mediated SiO_2NPs. The SEM image of PSA shown in Figure 5.3(a) shows heterogeneous materials with irregular shapes. A high roughness with particle sizes between 500 nm and 1 μm was observed, which indicated the release of organic matter from PSA after the combustion of PS. Here, the SEM image of the Pluronic mediated SiO_2NPs (Figure 5.3(b)) highlights a significant transformation in size as well as morphology compared to the PSA. In contrast to PSA, SiO_2NPs clearly showed a spherical shape with remarkably smaller particle sizes. The TEM image (Figure 5.3(c)) of SiO_2NPs also supported the shape of the nanoparticles, which are 18 nm in size. The result of SEM and TEM analyses indicate a successful extraction of the SiO_2NPs from PSA with the help of a Pluronic F127 polymer.

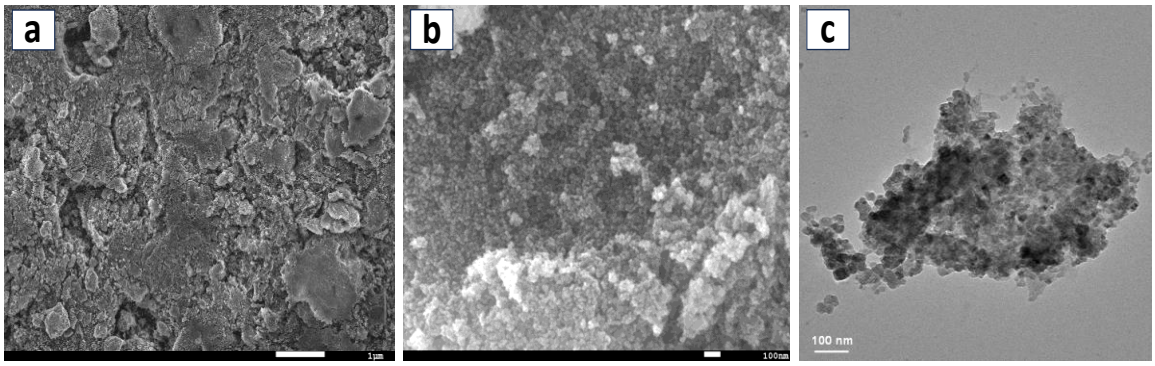

Figure 5.3: FE-SEM images of the (a) PSA (b) Pluronic mediated SiO_2NPs, and (c) TEM image of Pluronic mediated SiO_2NPs.

Therefore, this method for the development of SiO_2NPs, using a micellar environment of Pluronic, is very effective in reducing particle size and generating uniform morphology.

5.3.2: Characterization of Chitosan-modified SiO_2NPs (Ch/SiO_2NPs)

Combining chitosan and bio-based SiO_2NPs is a promising approach to developing newer adsorbents for various catalytic and biomedical applications [23, 34]. As shown in Scheme 5.1(b), various Ch/SiO_2NPs were synthesized by dissolving 10 gm of Pluronic mediated SiO_2NPs in a chitosan solution (0.5-2.0 g of chitosan in 100 mL of 2% acetic acid solution) with continuous stirring for 24 h. Chitosan was completely penetrated and homogenized throughout the pores of SiO_2NPs (mesoporous), and the mixture was centrifuged, filtered, washed with ultrapure water, and dried at 50 °C for 6 h, which resulted in a in a white powder of biosorbent Ch/SiO_2NPs.

The structural characterization of Ch/SiO_2NPs through DLS, FE-SEM, and TEM has been shown in Figure 5.4. The Pluronic mediated SiO_2NPs showed a hydrodynamic diameter of 22.3 nm and a negative zeta potential of -42 ± 3 mV (Figure 5.4 (a) and (b)).

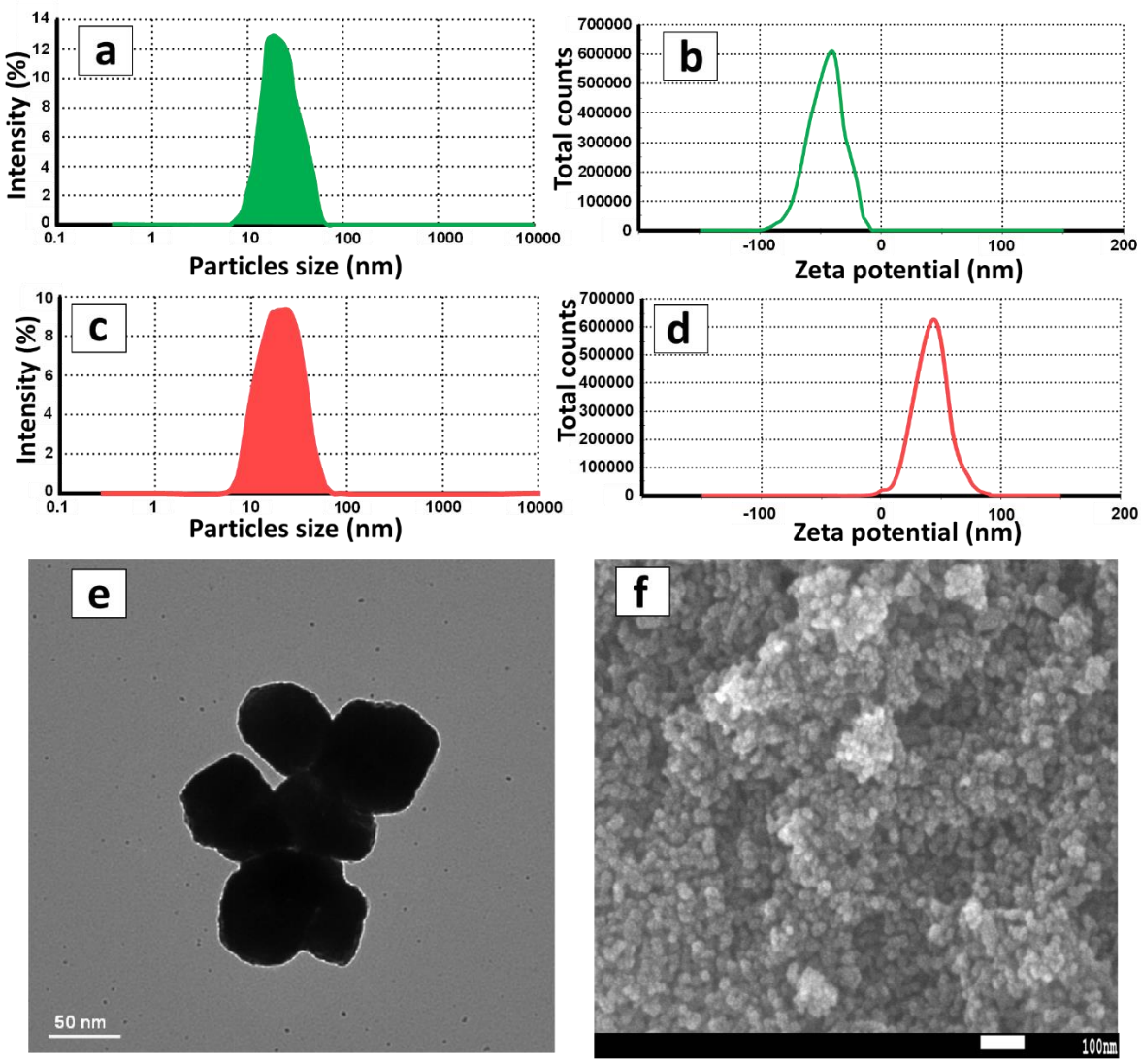

Figure 5.4: (a) Hydrodynamic diameter (D_h) of Pluronic mediated SiO_2NPs, (b) Zeta potential profile of Pluronic mediated SiO_2NPs, (c) Hydrodynamic diameter (D_h) of Ch/SiO_2NPs, (d) Zeta potential profile of Ch/SiO_2NPs, (e) TEM image, and (f) SEM image of Ch/SiO_2NPs biosorbent.

As shown in Figures 5.4(c) and 5.4(d), the biosorbent Ch/SiO_2NPs show hydrodynamic diameter sizes of 39.8 nm and a positive zeta potential value of 37 ± 2 mV, which are drastically different from the Pluronic mediated SiO_2NPs. The increment in hydrodynamic diameter showed that the size was increased after the chitosan coating. Also, the zeta potential shifting from a negative

value to a positive value clearly indicated the modification of chitosan over the surface of SiO_2NPs [34]. Figure 5.4(e) showed the TEM image of Ch/SiO_2NPs. It was clearly observed that the biosorbent consists of porous, spherical particles that are uniformly distributed, with an average size of 45.8 nm. In the TEM image of Ch/SiO_2NPs, the reduction in the porosity of nanoparticles was clearly seen which confirmed the modified SiO_2NPs with chitosan layers. The SEM image of Ch/SiO_2NPs (shown in Figure 5.4(f)) was also supported the TEM analysis as clearly spherical particles with uniformed distribution.

The XRD, FTIR and TGA characterization of biosorbent Ch/SiO_2NPs were presented in Figure 5.5(a) long with the comparison of Pluronic mediated SiO_2NPs and blank chitosan. The XRD pattern (Figure 5.5(a)) of the prepared SiO_2NPs showed a lower and broad peak at $2\theta=22.1°$, indicating the amorphous nature of nanoparticles [3]. The XRD curve of chitosan showed two broad peaks at $2\theta=9.1°$ and $2\theta=21.8°$, indicating its semicrystalline structure [35]. The XRD pattern of Ch/SiO_2NPs shows a minor diffraction peak at $2\theta=9.6°$ and a broad peak at $2\theta=22.2°$. Here, XRD pattern reveals that both pure chitosan and SiO_2NPs are similar. The decrease in crystallinity suggested that the bulky chitosan has been successfully coated onto the SiO_2NPs in biosorbent Ch/SiO_2NPs.

The FTIR spectrums of Pluronic mediated SiO_2NPs, chitosan and biosorbent Ch/SiO_2NPs are showed in Figure 5.5(b). The SiO_2NPs shows adsorption peaks at 3320 cm^{-1}(-OH stretching), 1625 cm^{-1}(-OH bending), 1101 cm^{-1}(Si-O bond stretching), 948 cm^{-1}(Si-OH bond stretching), 801 cm^{-1} (Si-O-Si bond stretching), and 463 cm^{-1}(Si-O-Si bond bending) [36]. In the FTIR spectrum of blank chitosan, the absorption peaks at 3442 cm^{-1}(–OH and N–H stretching), 2863 cm^{-1}(C–H stretching), 1652 cm^{-1}(amide C=O stretching), 1585 cm^{-1}(amideN–H stretching), 1315 cm^{-1}(amide C-Nstretching) 1092 cm^{-1}(C–O stretching 2°-OH), 1022 cm^{-1}(C–O bonds stretching1°-OH), and 886 cm^{-1}(C-O-C stretching). These results matched with reported values of chitosan [37]. The FTIR results of biosorbent Ch/SiO_2NPs shows adsorption peak at 3350 cm^{-1}(–OH stretching), 2886 cm^{-1}(C–H stretching), 1635 cm^{-1}(OH bending), 1360 cm^{-1}(CH_2bending), 1058 cm^{-1}(C–O–C stretching), 455 cm^{-1}(Si–O–Si bending). All the peaks clearly confirmed that the chitosan is attached to the SiO_2NPs. Additionally, the weaker absorption peak at 1635 cm^{-1} in Ch/SiO_2NPs compared to chitosan mainly indicated to the reduction in the hydrophilicity of the Ch/SiO_2NPs.

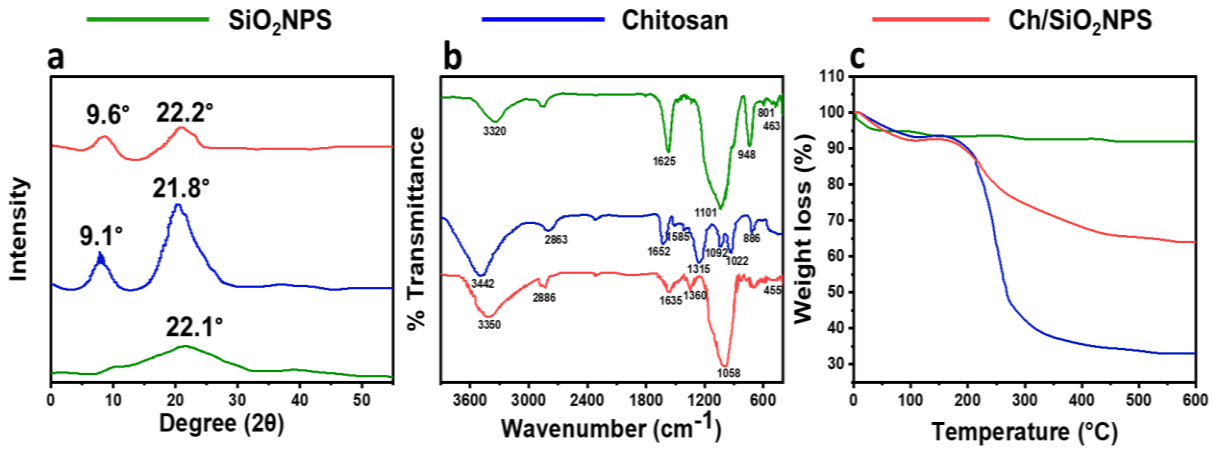

Figure 5.5: (a) XRD profile, (b) FTIR spectrum, and (c) TGA curves of Pluronic mediated SiO_2NPs, chitosan, and biosorbent Ch/SiO_2NPs.

Thermal properties and the impact of chitosan on Pluronic mediated SiO_2NPs were analyzed using TGA measurements (Figure 5.5(c)). TGA curve of SiO_2NPs shows a flat or nearly horizontal line, indicating that the nanoparticle remains stable and does not decompose up to 600°C. The weight loss of Ch/SiO_2NPs was found in three stages. The first stage weight loss (about 8%) below 100°C is attributed to the evaporation of physically absorbed moisture [38]. The following two stages of weight loss are associated with the dehydration and complete decomposition of molecular chains of chitosan [39]. As shown in Figure 7c, the residual weights at 600°C for SiO_2NPs (~92%) and Ch/SiO_2NPs (~63%) are higher than pure chitosan (~32%). Fast degradation occurs between 170°C and 400°C, followed by slower degradation from 400°C to 600°C, indicating the thermal degradation of coated chitosan molecules on SiO_2NPs surfaces. The higher residue at 600°C demonstrates the successful modification of SiO_2NPs with chitosan in Ch/SiO_2NPs.

As Ch/SiO_2NPs was synthesized with the purpose of being a biosorbent for adsorption of gases and the organic dye. Hence, the BET analysis is essential to know the surface area and porosity of the biosorbent. The N_2 sorption isotherms for Pluronic mediated SiO_2NPs and Ch/SiO_2NPs are displayed in Figure 5.6(a). Both samples (nanoparticles and biorsorbent) correspond to type IV isotherms and show a clear hysteresis loop in the high relative pressure, indicating the intake of mesoporosity in the system.

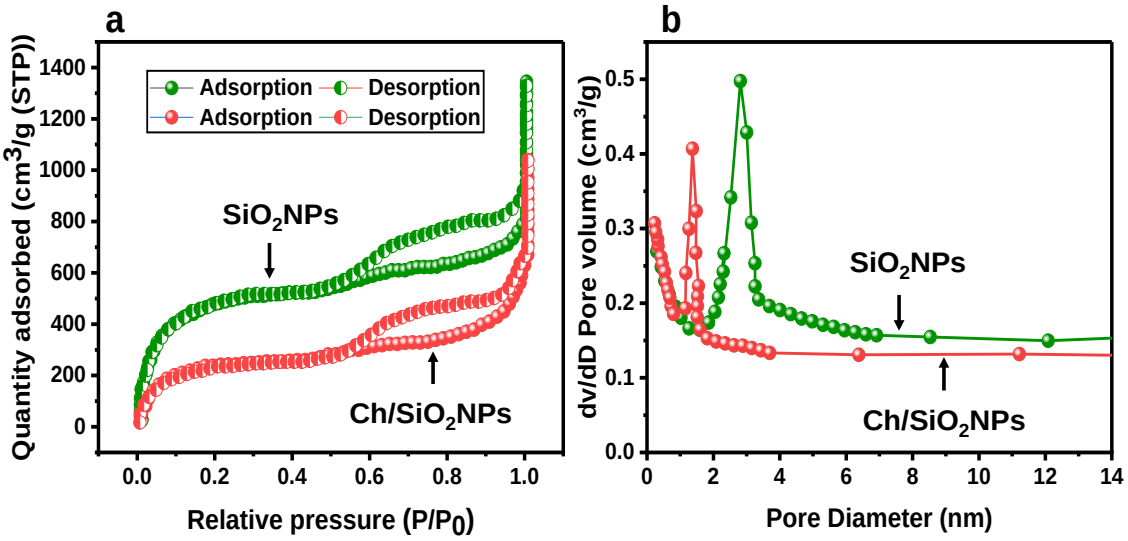

Figure 5.6: (a) N_2 adsorption-desorption isotherms and (b) Pore size distribution curves of Pluronic mediated SiO_2NPs and biosorbent Ch/SiO_2NPs.

As per the measurement, the pore volume of 1.38 cm^3/g and a surface area of 1089 m^2/g were found for SiO_2NPs, which decreased to 0.83 cm^3/g and 830 m^2/g for the biosorbent Ch/SiO_2NPs. Figure 5.6(b) shows a narrow pore size distribution, with SiO_2NPs at 2.79 nm and Ch/SiO_2NPs at 1.35 nm. The reduction in surface area, pore size, and pore volume in the Ch/SiO_2NPs clearly confirmed the incorporation of chitosan molecules on the surface and cavities of Pluronic mediated SiO_2NPs. Even after modification with chitosan, still Ch/SiO_2NPs have very effective pore size, pore volume, and surface area to utilize as the adsorbent for catalytic applications.

5.3.3: Gas adsorption study of Ch/SiO_2NPs biosorbents

5.3.3.1: Influence of chitosan content on SiO_2NPs in Ch/SiO_2NPs biosorbents

In general, chitosan shows a very low CO_2 adsorption because of its nonporous structure and smaller surface area [40]. Figure 5.7 shows the adsorption capacity of CO_2 gas on Pluronic mediated SiO_2NPs and various Ch/SiO_2NPs biosorbents. To understand the influence of chitosan content in the Ch/SiO_2NPs biosorbent for CO_2 adsorption, some parameters of textural properties were measured and listed in Table 5.3. Results showed that the SiO_2NPs adsorbed 0.21 mmol of CO_2 per gram, while various $Ch_{0.5}$/SiO_2NPs, $Ch_{1.0}$/SiO_2NPs, $Ch_{1.5}$/SiO_2NPs, and $Ch_{2.0}$/SiO_2NPs adsorbed 6.04, 6.70, 5.12, and 3.80 mmol/g, respectively.

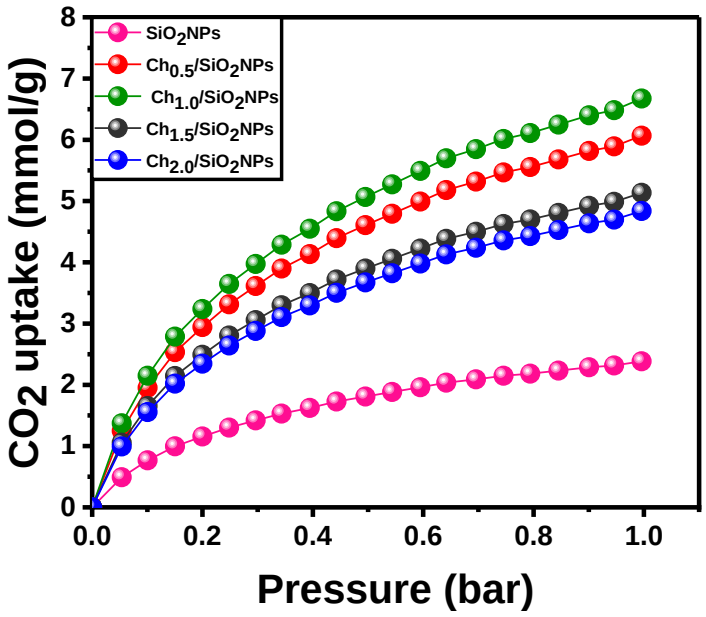

Figure 5.7: CO_2 adsorption capacity on different Ch/SiO_2NPs

Table 5.3: Compositions and textural properties of various Ch/SiO_2NPs biosorbents.

Adsorbent	Mass of Chitosan loaded to SiO_2NPs	Pore size (nm)	Pore volume (cm^3/g)	BET surfaces area (m^2/g)	CO_2 adsorption (mmol/g)
SiO_2NPs	-	2.79	1.38	1089	2.21
$Ch_{0.5}/SiO_2$NPs	0.5	1.66	0.95	943	6.04
$Ch_{1.0}/SiO_2$NPs	1.0	1.35	0.83	830	6.70
$Ch_{1.5}/SiO_2$NPs	1.5	0.42	0.52	616	5.12
$Ch_{2.0}/SiO_2$NPs	2.5	0.59	0.47	487	3.80

It was clearly found that when chitosan combined with SiO_2NPs in varying amounts, better adsorption of CO_2 was noticed compared to SiO_2NPs alone. Here, with increasing the amount of chitosan in the biosorbent, the pore size, volume, and surface area of mesoporous SiO_2NPs were decreased, but initially CO_2 adsorption was enhanced due to the availability of a high number of amino groups. While there was quite a high amount of chitosan (> 1.0 gm) in the biosorbent, the pores of silica nanospheres were occupied with chitosan molecules, which diminished the surface area of the biosorbent for CO_2 adsorption and showed not much enhancement of CO_2 adsorption (Figure 5.8).

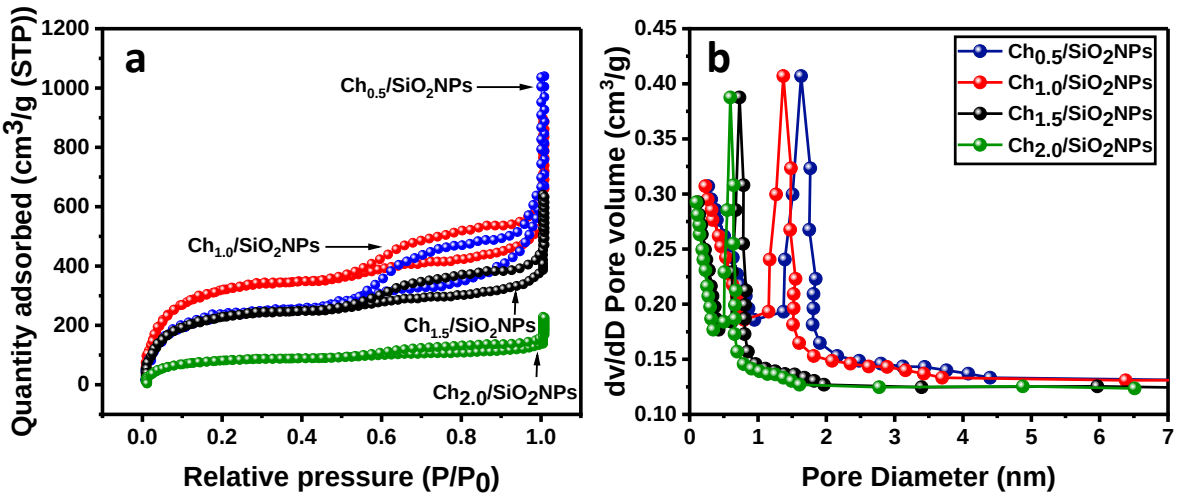

Figure 5.8: BET analysis of different biosorbents

After the CO_2 adsorption studies of Ch/SiO_2NPs with a varied amount of chitosan, it was clearly proved that the $Ch_{1.0}/SiO_2$NPs adsorbed a high amount of CO_2 (6.70 mmol/g) with a pore size of 1.35 nm, a pore volume of 0.83 cm^3/g, and a surface area of 830 m^2/g and found the best properties as a biosorbent for its further applications in adsorption of various gases and CR dye.

5.3.3.2: Adsorption of CO_2, CH_4, and N_2 gases on Ch/SiO_2NPs biosorbent

The adsorption of CO_2, CH_4, and N_2 gases on biosorbent $Ch_{1.0}/SiO_2$NPs at various temperatures is displayed in Figure 5.9(a–c). As per the results of the adsorption of various gases, CO_2 gets absorbed the most and N_2 is less at all the studied temperatures (shown in Figure 5.9 and Table 5.4). This occurs due to the physical properties of the gases. The critical temperatures for CO_2, CH_4, and N_2 are 30.85°, -83.15°C, and -147.15°C, respectively, following the order CO_2>CH_4>N_2 [41]. CO_2 is a linear, polar molecule with a significant quadrupole moment. This makes it interact more strongly with polar or hydrophilic surfaces like $Ch_{1.0}/SiO_2$NPs, which contain hydroxyl and amino groups from chitosan and silanol groups from SiO_2NPs. CO_2 can interact with basic sites on the biosorbent, such as amino groups in chitosan, leading to strong adsorption through acid-base interactions. CO_2 has a relatively small kinetic diameter (3.3 Å), allowing it to easily penetrate the pores of the biosorbent material [42]. CH_4 is non-polar and interacts with the adsorbent surface primarily through van der Waals forces, which are weaker than the interactions of polar molecules like CO_2. CH_4 has a larger kinetic diameter (3.8 Å) compared to CO_2, which can slightly hinder its access to the smaller pores within the biosorbent. Despite its larger size, CH_4can still be adsorbed through dispersion forces, but the overall

interaction strength is weaker than that of CO_2 [43]. N_2 is non-polar with a very small quadrupole moment, leading to the weakest interactions with the $Ch_{1.0}/SiO_2$NPs. N_2 has a kinetic diameter of 3.6 Å, but its non-polar nature results in weaker adsorption. The interactions between N_2 and the biosorbent surface are predominantly van der Waals forces, which are not as strong as the interactions between CO_2 and the biosorbent [44]. The adsorption order of CO_2>CH_4>N_2 on a $Ch_{1.0}/SiO_2$NPs is primarily due to the differences in molecular polarity, size, and interaction strength with the biosorbent's surface.

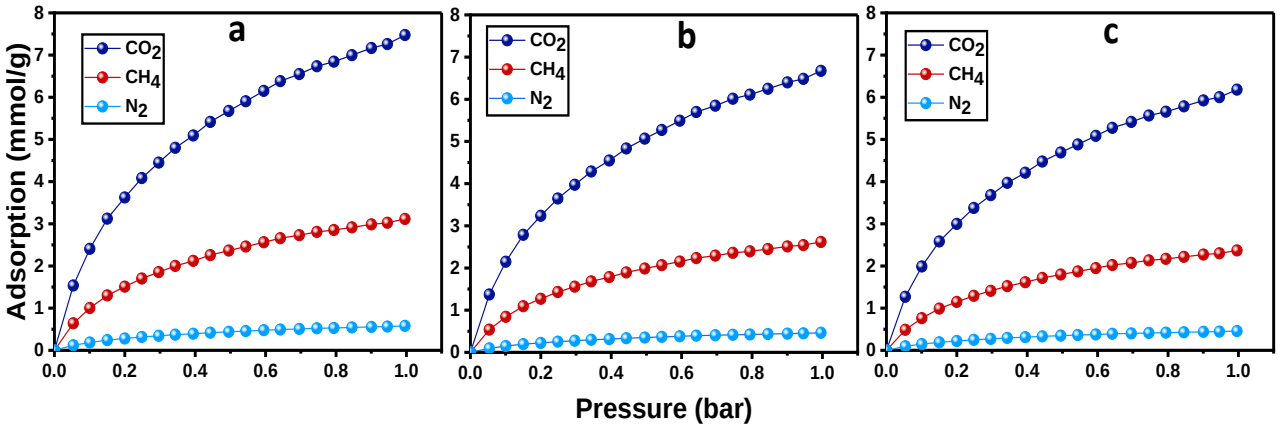

Figure 5.9: Gas adsorption isotherms on $Ch_{1.0}/SiO_2$NPs at (a) 15°C, (b) 25°C, and (c) 35°C.

It was also observed that the adsorption of these gases increased with an increase in the adsorptive pressure. With increasing pressure, there might be more effective interactions between gas and the $Ch_{1.0}/SiO_2$NPs as more gas molecules are available, leading to a slight increase in adsorption. Here, such an increase in adsorption may slow down as the surface becomes saturated. As shown in Table 5.4, the adsorption of gases on $Ch_{1.0}/SiO_2$NPs was reduced when the temperature was increased from 15°C to 35°C. At lower temperatures, the kinetic energy of the gas molecules reduces, allowing for stronger adsorption interactions with the surface of the biosorbent. At higher temperatures, gas molecules have higher kinetic energy, which weakens their interactions with the biosorbent surface [41].

Table 5.4: Amount of gas adsorbed on $Ch_{1.0}/SiO_2$NPs at different temperatures

Temperature °C	CO_2 mmol/g	CH_4 mmol/g	N_2 mmol/g
15	7.49	3.13	0.57
25	6.70	2.64	0.40
35	6.17	2.38	0.34

Figure 5.10 shows the adsorption kinetics of CO_2, CH_4, and N_2 gases in relation to the $Ch_{1.0}/SiO_2$NPs biosorbent sample at 25 °C. The selectivity (S) of adsorption gases for CO_2/CH_4, CH_4/N_2, and CO_2/N_2 was found to be 2.54, 6.50, and 16.50, respectively. Here, the rate of CO_2 adsorption was very fast and reached 6.7 mmol/g maximum within the 3 min. As per our results, $S_{CO_2/N_2}$is found far better than the other reported adsorbents, like sawdust-based porous carbon (S_{CO_2/N_2}=5.4) [45], microwave activated carbon (S_{CO_2/N_2}=15.0) [41], and activated template carbon (S_{CO_2/N_2}=6.5) [46].

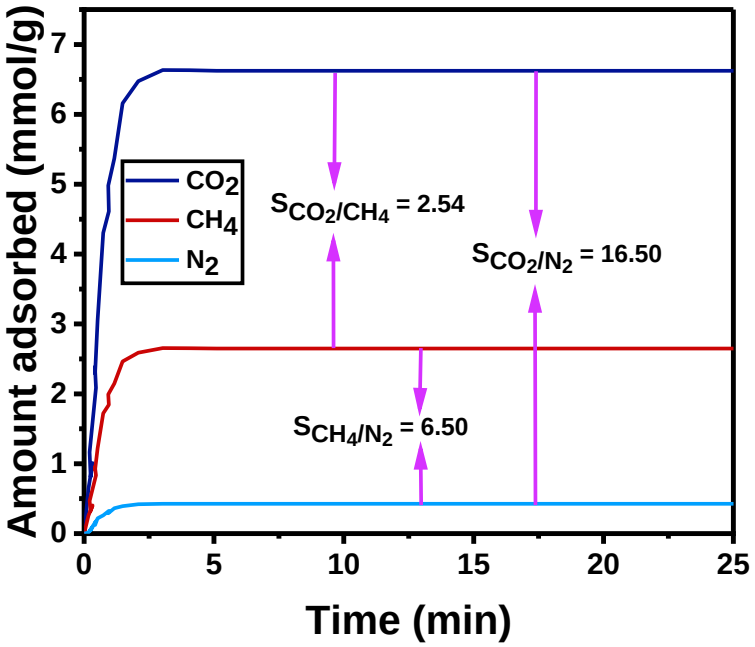

Figure 5.10: Selective separation of gas isotherm

5.4: References

1. Shahi, N., Wang, P., Adhikari, S., Min, B. and Rangari, V.K., 2021. Biopolymers fractionation and synthesis of nanocellulose/silica nanoparticles from agricultural byproducts. *ACS Sustainable Chemistry & Engineering*, *9*(18), pp.6284-6295.
2. Barhoum, A., Jeevanandam, J., Rastogi, A., Samyn, P., Boluk, Y., Dufresne, A., Danquah, M.K. and Bechelany, M., 2020. Plant celluloses, hemicelluloses, lignins, and volatile oils for the synthesis of nanoparticles and nanostructured materials. *Nanoscale*, *12*(45), pp.22845-22890.
3. Rovani, S., Santos, J.J., Corio, P. and Fungaro, D.A., 2018. Highly pure silica nanoparticles with high adsorption capacity obtained from sugarcane waste ash. *ACS omega*, *3*(3), pp.2618-2627.
4. Noor-ul-Amin, 2014. A multi-directional utilization of different ashes. *RSC Advances*, *4*(107), pp.62769-62788.
5. Vaibhav, V., Vijayalakshmi, U. and Roopan, S.M., 2015. Agricultural waste as a source for the production of silica nanoparticles. *Spectrochimica acta part A: Molecular and biomolecular spectroscopy*, *139*, pp.515-520.
6. Carmona, V.B., Oliveira, R.M., Silva, W.T.L., Mattoso, L.H.C. and Marconcini, J.M., 2013. Nanosilica from rice husk: extraction and characterization. *Industrial Crops and Products*, *43*, pp.291-296.
7. Yaro, S.A., Olajide, O.S., Asuke, F. and Popoola, A.P.I., 2017. Synthesis of groundnut shell nanoparticles: characterization and particle size determination. *The International Journal of Advanced Manufacturing Technology*, *91*, pp.1111-1116.
8. Peerzada, J.G. and Chidambaram, R., 2021. A statistical approach for biogenic synthesis of nano-silica from different agro-wastes. *Silicon*, *13*, pp.2089-2101.
9. Mandala, R., Hegde, G., Kodali, D. and Kode, V.R., 2023. From waste to strength: Unveiling the mechanical properties of peanut-shell-based polymer composites. *Journal of Composites Science*, *7*(8), p.307.
10. Arshadi, M., Attard, T.M., Lukasik, R.M., Brncic, M., da Costa Lopes, A.M., Finell, M., Geladi, P., Gerschenson, L.N., Gogus, F., Herrero, M. and Hunt, A.J., 2016. Pre-treatment

and extraction techniques for recovery of added value compounds from wastes throughout the agri-food chain. *Green Chemistry*, *18*(23), pp.6160-6204.

11. Mizutani, T., Arai, K., Miyamoto, M. and Kimura, Y., 2006. Application of silica-containing nano-composite emulsion to wall paint: A new environmentally safe paint of high performance. *Progress in Organic Coatings*, *55*(3), pp.276-283.
12. Vijayakumar, V. and Khastgir, D., 2018. Hybrid composite membranes of chitosan/sulfonated polyaniline/silica as polymer electrolyte membrane for fuel cells. *Carbohydrate polymers*, *179*, pp.152-163.
13. Zhao, S., Malfait, W.J., Demilecamps, A., Zhang, Y., Brunner, S., Huber, L., Tingaut, P., Rigacci, A., Budtova, T. and Koebel, M.M., 2015. Strong, thermally superinsulating biopolymer–silica aerogel hybrids by cogelation of silicic acid with pectin. *AngewandteChemie*, *127*(48), pp.14490-14494.
14. Wong, D.P., Suriyaprabha, R., Yuvakumar, R., Rajendran, V., Chen, Y.T., Hwang, B.J., Chen, L.C. and Chen, K.H., 2014. Binder-free rice husk-based silicon–graphene composite as energy efficient Li-ion battery anodes. *Journal of Materials Chemistry A*, *2*(33), pp.13437-13441.
15. Chen, F., Zhao, E., Kim, T., Wang, J., Hableel, G., Reardon, P.J.T., Ananthakrishna, S.J., Wang, T., Arconada-Alvarez, S., Knowles, J.C. and Jokerst, J.V., 2017. Organosilica nanoparticles with an intrinsic secondary amine: an efficient and reusable adsorbent for dyes. *ACS Applied Materials & Interfaces*, *9*(18), pp.15566-15576.
16. Nayab, S., Farrukh, A., Oluz, Z., Tuncel, E., Tariq, S.R., Rahman, H.U., Kirchhoff, K., Duran, H. and Yameen, B., 2014. Design and fabrication of branched polyamine functionalized mesoporous silica: an efficient absorbent for water remediation. *ACS applied materials & interfaces*, *6*(6), pp.4408-4417.
17. Joshi, D., Maurya, N.K., Kumar, N. and Mandal, A., 2022. Experimental investigation of silica nanoparticle assisted Surfactant and polymer systems for enhanced oil recovery. *Journal of Petroleum Science and Engineering*, *216*, p.110791.
18. Di Credico, B., Manzini, E., Viganò, L., Canevali, C., D'Arienzo, M., Mostoni, S., Nisticò, R. and Scotti, R., 2023. Silica nanoparticles self-assembly process in polymer composites: Towards advanced materials. *Ceramics International*, *49*(16), pp.26165-26181.

19. Rahman, I.A. and Padavettan, V., 2012. Synthesis of silica nanoparticles by sol-gel: size-dependent properties, surface modification, and applications in silica-polymer nanocomposites—a review. *Journal of nanomaterials*, *2012*(1), p.132424.
20. Meer, S., Kausar, A. and Iqbal, T., 2016. Attributes of polymer and silica nanoparticle composites: A review. *Polymer-Plastics Technology and Engineering*, *55*(8), pp.826-861.
21. Wang, J. and Zhuang, S., 2022. Chitosan-based materials: Preparation, modification and application. *Journal of Cleaner Production*, *355*, p.131825.
22. Rafigh, S.M. and Heydarinasab, A., 2017. Mesoporous chitosan–SiO_2 nanoparticles: synthesis, characterization, and CO_2 adsorption capacity. *ACS Sustainable Chemistry & Engineering*, *5*(11), pp.10379-10386.
23. Budnyak, T.M., Błachnio, M., Slabon, A., Jaworski, A., Tertykh, V.A., Deryło-Marczewska, A. and Marczewski, A.W., 2020. Chitosan deposited onto fumed silica surface as sustainable hybrid biosorbent for Acid Orange 8 dye capture: Effect of temperature in adsorption equilibrium and kinetics. *The Journal of Physical Chemistry C*, *124*(28), pp.15312-15323.
24. Rinaudo, M., 2006. Chitin and chitosan: Properties and applications. *Progress in polymer science*, *31*(7), pp.603-632.
25. Kalapathy, U., Proctor, A. and Shultz, J., 2000. A simple method for production of pure silica from rice hull ash. *Bioresource technology*, *73*(3), pp.257-262.
26. Alexandridis, P. and Tsianou, M., 2011. Block copolymer-directed metal nanoparticle morphogenesis and organization. *European Polymer Journal*, *47*(4), pp.569-583.
27. Sharma, R.K., Sharma, S., Dutta, S., Zboril, R. and Gawande, M.B., 2015. Silica-nanosphere-based organic–inorganic hybrid nanomaterials: synthesis, functionalization and applications in catalysis. *Green Chemistry*, *17*(6), pp.3207-3230.
28. Bodratti, A.M., Sarkar, B., Song, D., Tsianou, M. and Alexandridis, P., 2015. Competitive adsorption between PEO-containing block copolymers and homopolymers at silica. *Journal of Dispersion Science and Technology*, *36*(1), pp.1-9.
29. Uda, M.N.A., Gopinath, S.C., Hashim, U., Halim, N.H., Parmin, N.A., Afnan Uda, M.N. and Anbu, P., 2021. Production and characterization of silica nanoparticles from fly ash:

conversion of agro-waste into resource. *Preparative biochemistry & biotechnology*, *51*(1), pp.86-95.

30. Rovani, S., Santos, J.J., Corio, P. and Fungaro, D.A., 2019. An alternative and simple method for the preparation of bare silica nanoparticles using sugarcane waste ash, an abundant and despised residue in the Brazilian industry. *Journal of the Brazilian Chemical Society*, *30*, pp.1524-1533.
31. Akhayere, E., Vaseashta, A. and Kavaz, D., 2020. Novel magnetic nano silica synthesis using barley husk waste for removing petroleum from polluted water for environmental sustainability. *Sustainability*, *12*(24), p.10646.
32. Akhayere, E. and Kavaz, D., 2021. Nano-silica and nano-zeolite synthesized from barley grass straw for effective removal of gasoline from aqueous solution: a comparative study. *Chemical Engineering Communications*, *208*(10), pp.1419-1435.
33. Imoisili, P.E., Ukoba, K.O. and Jen, T.C., 2020. Green technology extraction and characterisation of silica nanoparticles from palm kernel shell ash via sol–gel. *Journal of Materials Research and Technology*, *9*(1), pp.307-313.
34. Buchman, J.T., Elmer, W.H., Ma, C., Landy, K.M., White, J.C. and Haynes, C.L., 2019. Chitosan-coated mesoporous silica nanoparticle treatment of Citrullus lanatus (watermelon): enhanced fungal disease suppression and modulated expression of stress-related genes. *ACS Sustainable Chemistry & Engineering*, *7*(24), pp.19649-19659.
35. Yen, M.T., Yang, J.H. and Mau, J.L., 2009. Physicochemical characterization of chitin and chitosan from crab shells. *Carbohydrate polymers*, *75*(1), pp.15-21.
36. Dubey, R.S., Rajesh, Y.B.R.D. and More, M.A., 2015. Synthesis and characterization of SiO2 nanoparticles via sol-gel method for industrial applications. *Materials Today: Proceedings*, *2*(4-5), pp.3575-3579.
37. Kasaai, M.R., 2008. A review of several reported procedures to determine the degree of N-acetylation for chitin and chitosan using infrared spectroscopy. *Carbohydrate polymers*, *71*(4), pp.497-508.
38. Lu, S., Duan, M. and Lin, S., 2003. Synthesis of superabsorbent starch-graft-poly (potassium acrylate-co-acrylamide) and its properties. *Journal of applied polymer science*, *88*(6), pp.1536-1542.

39. López, D., Cendoya, I., Torres, F., Tejada, J. and Mijangos, C., 2001. Preparation and characterization of poly (vinyl alcohol)-based magnetic nanocomposites. 1. Thermal and mechanical properties. *Journal of Applied Polymer Science*, *82*(13), pp.3215-3222.
40. Cmarik, G.E., Kim, M., Cohen, S.M. and Walton, K.S., 2012. Tuning the adsorption properties of UiO-66 via ligand functionalization. *Langmuir*, *28*(44), pp.15606-15613.
41. Yi, H., Li, F., Ning, P., Tang, X., Peng, J., Li, Y. and Deng, H., 2013. Adsorption separation of CO_2, CH_4, and N_2 on microwave activated carbon. *Chemical Engineering Journal*, *215*, pp.635-642.
42. Abd, A.A., Naji, S.Z., Hashim, A.S. and Othman, M.R., 2020. Carbon dioxide removal through physical adsorption using carbonaceous and non-carbonaceous adsorbents: a review. *Journal of Environmental Chemical Engineering*, *8*(5), p.104142.
43. Liu, H., Wang, S., Wang, X., Feng, X. and Chen, S., 2022. A stable solid amine adsorbent with interconnected open-cell structure for rapid CO_2 adsorption and CO2/CH4 separation. *Energy*, *258*, p.124899.
44. Hamyali, H., Nosratinia, F., Rashidi, A. and Ardjmand, M., 2022. Anthracite coal-derived activated carbon as an effectiveness adsorbent for superior gas adsorption and CO_2/N_2 and CO_2/CH_4 selectivity: Experimental and DFT study. *Journal of Environmental Chemical Engineering*, *10*(1), p.107007.
45. Sevilla, M. and Fuertes, A.B., 2011. Sustainable porous carbons with a superior performance for CO_2 capture. *Energy & Environmental Science*, *4*(5), pp.1765-1771.
46. Sevilla, M. and Fuertes, A.B., 2012. CO_2 adsorption by activated templated carbons. *Journal of colloid and interface science*, *366*(1), pp.147-154.